Fundamental drivers of dissolved organic matter composition across an Arctic effective precipitation gradient

Anne M. Kellerman [1]*, Ana Arellano,[2,a] David C. Podgorski,[1,b] Ellen E. Martin,[2] Jonathan B. Martin,[2] Kelly M. Deuerling,[2] Thomas S. Bianchi,[2] Robert G. M. Spencer[1]

[1]National High Magnetic Field Laboratory Geochemistry Group and Department of Earth, Ocean, and Atmospheric Science, Florida State University, Tallahassee, Florida
[2]Department of Geological Sciences, University of Florida, Gainesville, Florida

Abstract

The standard model for aquatic ecosystems is to link hydrologic connectivity to dissolved organic carbon (DOC) concentration and dissolved organic matter (DOM) composition and, ultimately, reactivity. Studies across effective precipitation gradients have been suggested as models for predicting how carbon cycling will change in Arctic aquatic ecosystems with projected drying (i.e., reduced hydrologic connectivity). To evaluate links between DOM dynamics and hydrologic connectivity, 41 stream samples from Greenland were analyzed across an effective precipitation gradient for DOM optical properties and elemental composition using ultrahigh-resolution mass spectrometry. Sites with negative effective precipitation and decreased hydrologic connectivity exhibited elevated specific conductivity (SpC) and DOC concentrations as well as DOM composition indicative of decreased hydrologic connectivity, for example, lower aromaticity, assessed using carbon-specific UV absorbance at 254 nm, decreased relative abundances of polyphenolic and condensed aromatic compounds, and increased relative abundances of highly unsaturated and phenolic compounds. Allochthonous inputs decreased as the summer progressed as exhibited by decreases in aromatic compounds. A decrease in molecular richness and N-containing compounds coincided with the decrease in allochthonous inputs. DOC concentrations increased over the summer but more slowly than SpC, suggesting degradation processes outweighed combined evapoconcentration and production. The patterns in DOM composition suggest evapoconcentration and photodegradation are dominant controls. However, when hydrologic connectivity was high, regardless of effective precipitation, DOM reflected allochthonous sources such as snowmelt-fed wetlands. These results highlight the challenges of modeling carbon cycling in aquatic ecosystems across effective precipitation gradients, particularly those with strong seasonality and regional variability in hydrologic inputs.

Dissolved organic matter (DOM) comprises a complex mixture of compounds from new production and degradation by-products from allochthonous and autochthonous sources. Allochthonous DOM originates from outside the aquatic system, typically from soil and litter, is enriched in aromatic structures, and exhibits high C/N ratios. Autochthonous DOM is internally produced usually by algae or macrophytes, is relatively enriched in aliphatics, and generally exhibits a low C/N ratio (Findlay and Sinsabaugh 2003; Kellerman et al. 2018). DOM has a multifunctional role in aquatic ecosystems; for example, DOM is the base of the microbial food web (Pace et al. 2004), binds and affects the reactivity of metals (Aiken et al. 2011), and protects aquatic fauna from UV radiation (Molot et al. 2004). DOM composition has been linked to reactivity and ultimately its fate in the environment (Sun et al. 1997; Stubbins et al. 2010; Kellerman et al. 2015). Despite regional variance, dissolved organic carbon (DOC) concentration covaries globally with chromophoric DOM (CDOM; e.g., absorbance at 350 nm) (Massicotte et al. 2017). In boreal and Arctic systems, DOC concentrations and CDOM are often tightly linked due to dominant allochthonous inputs (Spencer et al. 2009; Stedmon et al. 2011; Kothawala et al. 2014; Mann et al. 2016), characterized by high carbon-specific UV absorbance at 254 nm ($SUVA_{254}$), a proxy for aromaticity determined by ^{13}C NMR (Weishaar et al. 2003).

*Correspondence: akellerman@fsu.edu

Additional Supporting Information may be found in the online version of this article.

Present address:
[a]College of Marine Science, University of South Florida, Saint Petersburg, Florida
[b]Pontchartrain Institute for Environmental Sciences, Department of Chemistry, University of New Orleans, New Orleans, Louisiana

Aquatic ecosystems in semiarid environments typically exhibit elevated DOC concentrations and low $SUVA_{254}$ values, a deviation from the global positive association found between DOC concentration and CDOM content (Curtis and Adams 1995; Anderson and Stedmon 2007; Osburn et al. 2011; Bogard et al. 2019). This relationship has been postulated to be due to the hydrologic disconnection between these aquatic systems and their catchments, where soil water does not interact with surface waters that enter streams and lakes (Good et al. 2015). In regions with low precipitation and high rates of evapotranspiration, low amounts of runoff limit the mobilization of DOM and nutrients from the catchment to aquatic systems (i.e., low connectivity = limited new allochthonous inputs). Additionally, limited runoff, low precipitation, and high evapotranspiration result in increasing water residence times in semiarid systems, allowing more time for photodegradation and in situ production of DOM (Osburn et al. 2011; Saros et al. 2015). The extent of hydrologic disconnection and evaporation can be evaluated using stable water isotopes; $\delta^{18}O$ becomes enriched faster than δD due to evaporation, resulting in a local evaporation line (LEL) with a lower slope than the Global Meteoric Water Line (Craig 1961; Brooks et al. 2014; Good et al. 2015). Effective precipitation (the difference between precipitation and evapotranspiration) is negative near the Greenland Ice Sheet (-150 mm yr^{-1}) and positive near the coast ($+150$ mm yr^{-1}) (Hasholt and Søgaard 1978). Thus, drainage from the deglaciated watersheds in western Greenland is controlled by an effective precipitation gradient, making it an ideal location to study the controls of DOC concentration and DOM composition across hydrologic regimes in the Arctic (Osburn et al. 2017).

Little is known about how DOM is produced and processed in these watersheds. Decreases in DOC concentrations over the past decade have been linked to increases in soil ionic strength (Saros et al. 2015), which suggests DOC concentration is controlled by allochthonous inputs, and the associated low CDOM content is a result of photobleaching and microbial degradation rather than autochthonous production. Alternatively, a decrease in terrestrial inputs could allow for autochthonous production to dominate the DOM pool. Weak connectivity between aquatic systems and their catchments could result in higher autochthonous contributions particularly as the summer season progresses, potentially from benthic production, which has been found to account for > 80% of primary production in shallow oligotrophic lakes in Greenland (Vadeboncoeur et al. 2003). However, high contributions of benthic primary production is typical of Arctic lakes with low DOC concentrations and low CDOM (Ask et al. 2009), whereas lakes in semiarid western Greenland exhibit elevated DOC concentrations with relatively low CDOM content (Anderson and Stedmon 2007).

DOM is the most important intermediary in the global carbon cycle (Battin et al. 2009) and comprises 83% ± 11% of the organic matter pool exported from Arctic rivers (McClelland et al. 2016). Linking DOM composition to sources and processing has been a major goal of DOM biogeochemistry since the 1990s (e.g., Sun et al. 1997; McKnight et al. 2001). The source and degree of processing of DOM can be inferred using absorbance and fluorescence characteristics; however, deducing DOC concentrations and DOM sources from optical properties can be problematic in systems with long water residence times (Helms et al. 2008; Fellman et al. 2010). For example, the weak relationship between DOC concentration and CDOM in the St. Lawrence River is due to long residence times in the Laurentian Great Lakes, which allows for extended DOM processing and increased inputs of DOM from in situ production, and renders estimating DOC concentration from CDOM inappropriate (Spencer et al. 2012). Advances in data processing have allowed the application of ultrahigh-resolution Fourier transform ion cyclotron resonance mass spectrometry (FT-ICR MS) to environmental data sets where we can link DOM composition to sources and processing. Polyphenolic and condensed aromatic compounds are linked to terrestrial sources (Kellerman et al. 2014, 2018) and are particularly susceptible to photodegradation (Gonsior et al. 2009; Stubbins et al. 2010). Microbial and algal production of DOM has been linked to aliphatic, N- and S-containing compounds (Osterholz et al. 2016; Noriega-Ortega et al. 2019). Microbial communities are capable of degrading several types of compounds with a preference for energy-rich aliphatic compounds (D'Andrilli et al. 2015; Spencer et al. 2015; Mostovaya et al. 2017).

In this study, we examine the sources of DOM across an effective precipitation gradient in western Greenland and throughout a summer season using optical properties and FT-ICR MS. We utilize widely accessible, inexpensive, and high-throughout optical analyses in conjunction with ultrahigh resolution mass spectra analyses, to assess the detailed molecular composition of DOM beyond changes in aromaticity. Additionally, this is the first study to assess the detailed molecular composition of DOM in these atypical aquatic ecosystems of southwest Greenland. We establish whether the high DOC concentrations and low $SUVA_{254}$ values that occur in regions with negative effective precipitation result: (1) from the photobleaching and photo-enhanced biodegradation of terrestrial DOM; or (2) from the production of relatively aliphatic and heteroatomic enriched autochthonous DOM. We aim to establish a link between detailed molecular composition and effective precipitation and hypothesize that aquatic ecosystems in regions with negative effective precipitation will be the least aromatic (assessed using $SUVA_{254}$, and FT-ICR MS derived polyphenolic and condensed aromatic compound groups) and decrease throughout the summer, as allochthonous inputs decrease and evapoconcentration extends residence times allowing for ongoing photodegradation and additional in situ production. Furthermore, we hypothesize that DOM in regions with positive effective precipitation will have higher aromaticity, indicating greater delivery of allochthonous DOM

due to greater hydrologic connectivity. However, we expect sites that exhibit seasonal variability in hydrologic connectivity to deviate from these patterns, with high aromaticity and high DOC concentrations, as snowmelt connects DOM-rich wetlands at the onset of summer. Ultimately, delineating sources and processing of DOM across an effective precipitation gradient is required for understanding how aquatic ecosystems will respond to ongoing climate change.

Methods

Sampling sites and sample collection

Stream samples were collected between 05 June 2013 and 30 July 2013 (n = 41), 10 of which were taken from lake outlets, across five regions between Sisimiut (66.94°N, 53.67°W) on the west coast of Greenland to Isunngua (67.01°N, 50.69°W) near the ice sheet (Fig. 1; Table 1). All watersheds are disconnected from the Greenland Ice Sheet by a hydrologic divide. The area is underlain by Archean orthogneisses of the Nagssugtoqidian Mobile Belt and covered by shrubby vegetation and grasses, which increase toward the coast where precipitation is higher.

Sampling regions were grouped a priori into two categories based on regional effective precipitation, where the inland sites (Qorlortoq, Lake Helen, and Isunngua; GL1–GL31; Fig. 1; Table 1) and the coastal sites (Sisimiut and Nerumaq; GL32–GL41; Fig. 1; Table 1) experience negative and positive effective precipitation, respectively. The boundary between positive and negative effective precipitation occurs ~ 52°W, halfway between the coast and the ice sheet (Hasholt and Søgaard 1978; Anderson et al. 2001). Sites with negative effective precipitation receive ~ 150 mm yr^{-1} of precipitation and lose ~ 300 mm yr^{-1} through evapotranspiration (GL1–GL31). Sites with positive effective precipitation receive ~ 300 mm yr^{-1} of precipitation

and lose ~ 150 mm yr^{-1} through evapotranspiration (GL32–GL41). Samples were collected three times throughout the summer to assess temporal impacts of negative effective precipitation on DOC concentration and DOM composition in the Lake Helen (n = 4) and Isunngua regions (n = 1).

The detailed sampling protocol is described in Scribner et al. (2015). Briefly, a YSI Pro Plus sonde was used to measure water temperature, pH, dissolved oxygen, and specific conductivity (SpC). Filtered water (0.45 μm trace metal grade Geotech dispos-a-filter Versapor® filter capsules) was collected for water isotopes, DOC concentration, and DOM composition. Samples for DOC and DOM analyses were collected in muffled amber glass bottles and DOC samples were acidified with HCl to pH 2 and stored at 4°C in the dark.

Water isotopes

Water isotopes (δD and $\delta^{18}O$) were measured using a Picarro L2120-I Isotopic Liquid Water & Certified Continuous Water Vapor Analyzer with a Picarro A0211 High Precision Vaporizer and CTC HTS PAL autosampler. Results are reported as per mil compared to Vienna Standard Mean Ocean Water (VSMOW). Repeated analyses of an in-house standard had a coefficient of variance of 4% for $\delta^{18}O$ and 8% for δD.

DOC concentration and DOM optical characterization

DOC concentrations were measured by high-temperature catalytic oxidation using a Shimadzu TOC-V$_{CSH/CSN}$ (Guo et al. 1994). DOC concentration measurements were bracketed with standard curve measurements and crosschecked against a deep seawater reference (Carbon Reference Materials, University of Miami, Rosenstiel School of Marine and Atmospheric Sciences). Reported DOC concentrations are the mean of three
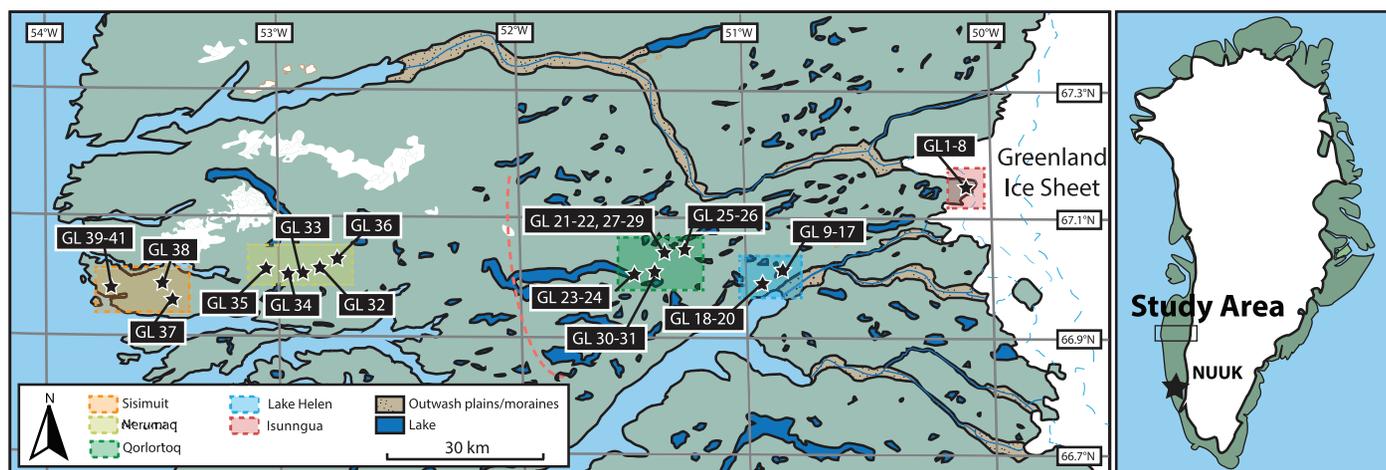
Fig. 1. Map of sampling locations west of the Greenland Ice Sheet. Sites that were sampled in time series or where the markers would overlap are indicated by sample numbers in the white lined black boxes. The transition from west to east between positive (Sisimiut and Nerumaq) to negative precipitation (Qorlortoq, Lake Helen, and Isunngua) occurs at approximately 52°W (dotted line as per Anderson et al. 2001). In the online version, colored boxes denote the sampling regions. [Color figure can be viewed at wileyonlinelibrary.com]

Table 1. Site names, location, sampling dates, coordinates, and evaporative conditions for sample sites

Sample name	Region	Date	Latitude	Longitude	Specific conductivity (μS cm^{-1})	δ^{18}O ‰*	δD ‰*
GL1	Isunngua[I]	05 Jun 13	67.1496	−50.0666	31.7	−18.7	−140.1
GL2	Isunngua[I]	13 Jul 13	67.14962	−50.06663	88.3	−11.8	−116.8
GL3	Isunngua[I]	30 Jul 13	67.14962	−50.06662	111.4	−11.8	−118.3
GL4	Isunngua	05 Jun 13	67.14846	−50.06752	74.4	−18.0	−138.9
GL5	Isunngua	05 Jun 13	67.14771	−50.06752	75.1	−18.1	−139.2
GL6	Isunngua	05 Jun 13	67.14393	−50.06755	80.8	−18.2	−139.8
GL7	Isunngua	08 Jun 13	67.15203	−50.08381	66.8	−16.0	−130.9
GL8	Isunngua	08 Jun 13	67.14869	−50.07993	57	−17.3	−137.0
GL9	Lake Helen[II]	09 Jun 13	67.02335	−50.82552	55.4	−11.6	−108.0
GL10	Lake Helen[II]	12 Jul 13	67.02341	−50.82574	102.3	−10.2	−101.3
GL11	Lake Helen[II]	28 Jul 13	67.02341	−50.82575	115.2	−10.1	−101.6
GL12	Lake Helen[III]	09 Jun 13	67.01692	−50.8562	75	−12.5	−111.1
GL13	Lake Helen[III]	12 Jul 13	67.0156	−50.86085	124.7	−11.3	−107.3
GL14	Lake Helen[III]	28 Jul 13	67.0156	−50.86085	180	−12.2	−111.3
GL15	Lake Helen[IV]	09 Jun 13	67.00815	−50.87608	110.7	−12.1	−110.2
GL16	Lake Helen[IV]	12 Jul 13	67.00816	−50.87609	133.3	−11.5	−107.4
GL17	Lake Helen[IV]	28 Jul 13	67.00816	−50.87609	162.6	−12.0	−110.4
GL18	Lake Helen[V]	11 Jun 13	66.98958	−50.93108	107.4	−10.7	−103.8
GL19	Lake Helen[V]	12 Jul 13	66.98944	−50.93128	198.2	−11.0	−106.3
GL20	Lake Helen[V]	28 Jul 13	66.98943	−50.93122	257.6	−13.1	−116.1
GL21	Qorlortoq	22 Jul 13	67.03515	−51.36023	183.2	−10.0	−98.6
GL22	Qorlortoq	22 Jul 13	67.02866	−51.36569	212.9	−10.0	−97.9
GL23	Qorlortoq	21 Jul 13	67.01822	−51.43164	243.9	−9.9	−98.4
GL24	Qorlortoq	21 Jul 13	67.0089	−51.46678	373.6	−9.5	−96.8
GL25	Qorlortoq	19 Jul 13	67.03016	−51.28801	191.4	−15.4	−122.4
GL26	Qorlortoq	19 Jul 13	67.033	−51.28466	194.3	−14.9	−119.6
GL27	Qorlortoq	20 Jul 13	67.03957	−51.34821	215	−9.8	−98.3
GL28	Qorlortoq	20 Jul 13	67.0525	−51.33503	150.2	−9.8	−97.3
GL29	Qorlortoq	20 Jul 13	67.04418	−51.34759	158.4	−9.9	−98.1
GL30	Qorlortoq	21 Jul 13	67.01581	−51.39448	301.9	−10.6	−100.3
GL31	Qorlortoq	23 Jul 13	67.0107	−51.36922	451.8	−9.4	−94.7
GL32	Nerumaq	30 Jun 13	67.01157	−52.86885	120.5	−15.8	−117.5
GL33	Nerumaq	30 Jun 13	67.0049	−52.9128	123.3	−15.8	−117.3
GL34	Nerumaq	02 Jul 13	67.00509	−52.96457	118	−15.8	−116.7
GL35	Nerumaq	01 Jul 13	67.01607	−53.03032	100.4	−15.9	−116.5
GL36	Nerumaq	26 Jun 13	67.02617	−52.79885	46.8	−16.1	−118.5
GL37	Sisimiut	18 Jun 13	66.9501	−53.45262	31.2	−15.0	−107.9
GL38	Sisimiut	23 Jun 13	66.97227	−53.4867	56.6	−14.8	−107.8
GL39	Sisimiut	19 Jun 13	66.96763	−53.67804	38.9	−14.6	−102.1
GL40	Sisimiut	19 Jun 13	66.9641	−53.67577	45.8	−14.6	−102.5
GL41	Sisimiut	19 Jun 13	66.95554	−53.69738	48	−14.4	−101.8

Roman numerals indicate the sites sampled in a time series where numerals correspond to red numerals (I), orange (II), green (III), blue (IV), and purple (V) numbers in the online color versions of Figures 2–4 and 6–8.
*δ^{18}O ‰ and δD ‰ are calculated as the deviation between sample water isotopes in comparison to Vienna Standard Mean Ocean Water in per mil (‰).

replicate injections with a coefficient of variance of less than 2% (Mann et al. 2012).

Absorbance spectra were collected from 200 to 600 nm on a Shimadzu UV-1800 spectrophotometer using a 1-cm quartz cuvette. An indicator of the aromaticity of bulk DOM, SUVA$_{254}$ (Traina et al. 1990), was calculated as the absorbance per meter at 254 nm normalized to DOC concentration (mg C L^{-1}) and was corrected for absorbance from iron (Weishaar et al. 2003; Poulin et al. 2014). Spectral slopes were calculated by fitting an exponential equation to the

absorption spectra between 275–295 nm and 350–400 nm using:

$$\alpha(\lambda) = \alpha(\lambda_{\text{ref}})e^{-S(\lambda - \lambda_{\text{ref}})} \tag{1}$$

where $\alpha(\lambda)$ is the absorption coefficient of CDOM at a specified wavelength, λ_{ref} is a reference wavelength, and S is the slope fitting parameter (Helms et al. 2008; Spencer et al. 2012). The slope ratio (S_R) was calculated as the ratio of the two spectral slopes and has been linked to molecular weight and aromaticity of DOM (Helms et al. 2008).

Excitation emission matrices (EEMs) were collected using a Hitachi F-7000 fluorescence spectrophotometer across the emission range of 260–600 nm at 2 nm increments and excitation wavelengths from 250 to 455 nm at 5 nm increments. Excitation and emission slit widths were 5 nm and 2.5 nm, respectively. EEMs were corrected for instrument specific bias and inner filter effects using the drEEM toolbox for MATLAB (Murphy et al. 2013). A four-component model was elucidated using parallel factor analysis (PARAFAC) modeling and validated using the split-half technique and by comparing spectra from calibration and validation data sets (Supporting Information Fig. S1). We report the relative contribution of each PARA-FAC component (i.e., percent of each component), a useful metric for assessing optical properties of DOM, independent of DOC concentration (Fellman et al. 2010; Kothawala et al. 2014).

Fourier transform ion cyclotron resonance mass spectrometry

DOM was solid-phase extracted (SPE) to a target concentration of 40 μg C mL^{-1}. SPE extractions were per Dittmar et al. (2008) with the following modifications: 100 mg cartridges (Agilent, Bond Elut PPL) were rinsed with high performance liquid chromatography (HPLC) grade methanol, then left to soak overnight containing methanol. Cartridges were drained, rinsed with ultrapure water, methanol, and conditioned with pH 2 ultrapure water. Acidified samples were passed through cartridges based on DOC concentration; the volume ranged from 1.7 to 57 mL of sample. Cartridges were rinsed with pH 2 ultrapure water and dried with N$_2$ gas. Samples were eluted with methanol into precombusted amber glass vials and stored at -20°C until analysis. Samples were analyzed on a custom-built FT-ICR MS equipped with a passively shielded 9.4 T magnet (Oxford Instruments, Abingdon, Oxfordshire, U.K.) at the National High Magnetic Field Laboratory (Tallahassee, FL, U.S.A.; Stenson et al. 2003; Kaiser et al. 2011). Negatively charged ions were produced with electrospray ionization and infused directly at a flow rate of 700 nL min^{-1}. Needle voltage was -2500 V. Each mass spectrum was the sum of 100 transients.

Molecular formulae were assigned using previously described guidelines (Koch et al. 2007) to peaks with intensity > 6σ root mean square baseline noise, using the in-house software EnviroOrg©™. For this data set, 28,284 formulae were

assigned within the molecular bounds of $C_{1-45}H_{1-92}N_{0-4}O_{1-25}S_{0-2}$. Relative abundance was calculated as the percent of each peak to the total signal of all peaks in a sample. Molecular formulae were classified based on elemental ratios and modified aromaticity index (AI$_{\text{mod}}$) (Koch and Dittmar 2006, 2016). AI$_{\text{mod}}$ was calculated for each formula using the equation:

$$\text{AI}_{\text{mod}} = \frac{\text{DBE}_{\text{AI}}}{C_{\text{AI}}} = \frac{1 + C - \frac{1}{2}O - S - \frac{1}{2}(N+H)}{C - \frac{1}{2}O - N - S} \tag{2}$$

where C, H, O, N, and S correspond to the number of atoms of each element in a formula, and only applies when DBE$_{\text{AI}}$ and C_{AI} are greater than zero (Koch and Dittmar 2016). Compound categories were delineated by the following cutoffs: polycyclic and condensed aromatic compounds (AI$_{\text{mod}}$ > 0.66), polyphenolic compounds (0.66 $\geq$ AI$_{\text{mod}}$ > 0.5), highly unsaturated and phenolic compounds (AI$_{\text{mod}}$ < 0.5 and H/C < 1.5), aliphatic compounds (2 $\geq$ H/C $\geq$ 1.5, $N = 0$, O/C $\leq$ 0.9), N-containing aliphatic compounds (2 $\geq$ H/C $\geq$ 1.5, $N > 0$, O/C $\leq$ 0.9), or sugar-like compounds (H/C $\geq$ 1.5, O/C > 0.9; Rossel et al. 2015). Molecular formulae describe FT-ICR MS detected peaks of dissolved organic molecules but can represent numerous structural isomers (Hertkorn et al. 2007). The use of the term "compound" refers to the compounds the molecular formulae represent, not a particular structural isomer, and is only used in reference to compound categories. N-containing aliphatics and sugar-like compounds only exceeded 1% of the relative abundance in one sample each, and are not discussed.

Statistical analyses

Statistical analyses were carried out in R (R Core Team 2015). Data were tested for heteroscedasticity using the studentized Breusch-Pagan test. If data were heteroscedastic, a log$_{10}$ transformation, Box-Cox transformation, or a Welch's t-test that does not assume equal variances was applied. For statistical tests, $n = 41$, except for the time series analyses, where $n = 15$ (five sites were sampled in early June, early July, and late July). Spearman rank correlation coefficients were calculated between the relative abundance of molecular formulae in each sample and SpC using the "Hmisc" package (Harrell 2016). Nonmetric multidimensional scaling (NMDS) was conducted using the "vegan" package (Oksanen et al. 2011) on variables that were scaled to a range of 0–1. Relationships were considered significant with a false discovery rate (Benjamini and Hochberg 1995) corrected $p < 0.05$. To compare the change in the ratio of DOC concentration to SpC throughout the course of the summer in the five sites sampled in a time series, site-specific standard scores (z-scores) were calculated for the ratio of DOC concentration and SpC. This was done to isolate the temporal changes from site-specific values. The site-specific z-scores were calculated by centering to 0 and standardizing to a standard deviation (SD) of 1, where the

average DOC concentration to SpC ratio at each site was subtracted from the individual observations, then divided by the site-specific SD.
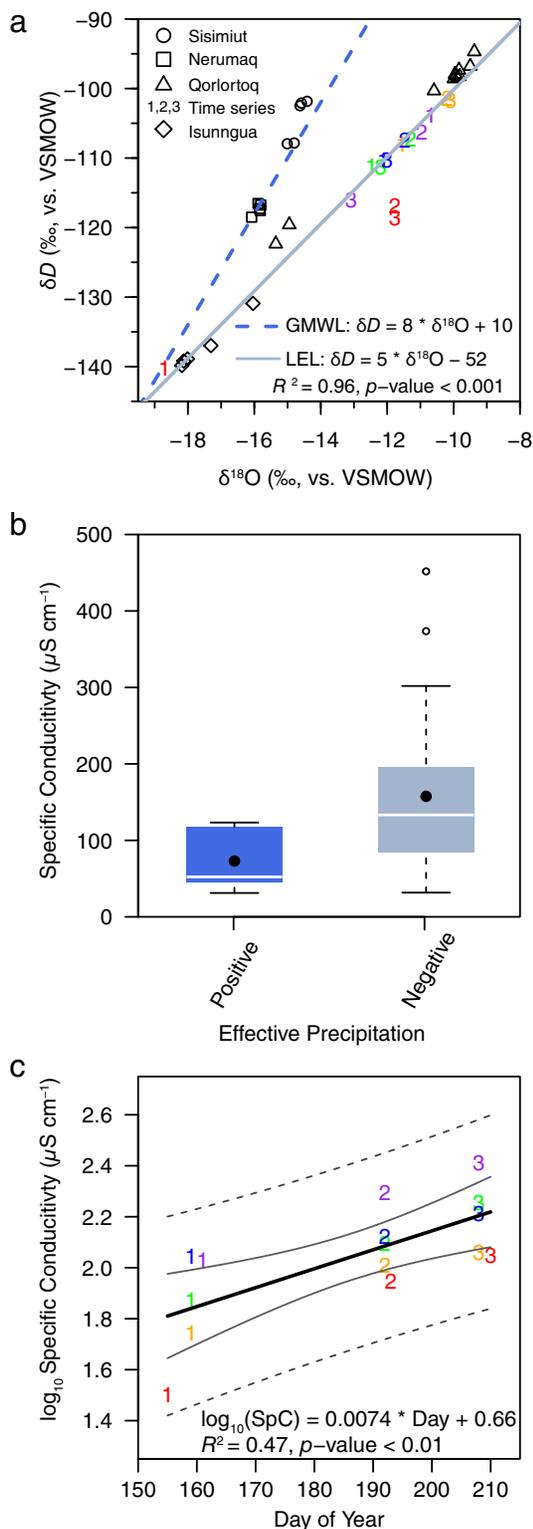
Results

Evaporative conditions of aquatic ecosystems in West Greenland

Water isotopes confirm the a priori-defined negative and positive effective precipitation sites. Sites with positive effective precipitation exhibit water isotopes that fall along the Global Meteoric Water Line (Fig. 2a), whereas sites with negative effective precipitation exhibit a clockwise shift away from the Global Meteoric Water Line, reflecting evaporation. Isunngua sites (red 1 and black diamonds in Fig. 2a) may seem to fall on either line, but samples taken later in the season (red 2 and 3) fall along the LEL of the region with negative effective precipitation, a result of evaporation during the summer. This is typical of inundated aquatic systems during freshet and the LEL is similar to that previously established for the region (Leng and Anderson 2003; Gibson et al. 2008). This site (red 1, 2, and 3 in Fig. 2c) exhibited the greatest seasonal change of the sites sampled in a time series.

SpC was highly variable with a mean $\pm$ SD of 136.9 $\pm$ 92.1 μS cm^{-1} (Table 1). Sites with positive effective precipitation (GL32–GL41; $n = 10$; Fig. 1) exhibited lower and less variable SpC (73.0 $\pm$ 37.7 μS cm^{-1}) than sites with negative effective precipitation (157.6 $\pm$ 95.3 μS cm^{-1}; $n = 31$; GL1–GL31; Fig. 2b; $p < 0.001$). SpC increased over the course of the summer season in sites where samples were taken in a time series ($R^2 = 0.44$, $p < 0.01$, $n = 15$; Fig. 2c), reflecting the evapoconcentrative effects of negative effective precipitation.

DOC concentration and DOM optical characteristics

DOC concentrations ranged from 1.02 to 32.05 mg L^{-1} (mean $\pm$ SD: 11.50 $\pm$ 7.43 mg L^{-1}; Table 2). Sites with positive effective precipitation exhibited lower and less variable DOC concentrations (2.04 $\pm$ 0.72 mg L^{-1}) than sites with negative effective precipitation (14.56 $\pm$ 5.82 mg L^{-1}; $t(32.7) = 11.7$, $p < 0.001$; Fig. 3a). Box-Cox transformed DOC concentration

Fig. 2. Extent of evapoconcentration in aquatic systems west of the Greenland Ice Sheet. (**a**) Water isotopes (δD against $\delta^{18}O$ ‰, vs. VSMOW) exhibit samples came from sites with two distinct hydrologic regimes. The dashed line indicates the Global Meteoric Water Line described by the equation $\delta D = 8.0 * \delta^{18}O + 10$. The LEL (solid line) equation is calculated from samples with negative effective precipitation. (**b**) SpC was lower in regions with positive effective precipitation than negative and (**c**) increased over time at sites sampled in a time series. In panel (**c**), the black line represents the regression line, the solid gray and dashed gray lines represent the 95% confidence and prediction intervals, respectively. In panels (**a**, **c**), symbols indicate the site and numbers indicate sites sampled in time series. Sisimiut (circles) and Nerumaq (squares) regions have positive effective precipitation, whereas Qorlortoq (triangles), Lake Helen and Isunngua (numbers and black diamonds) regions have negative effective precipitation. Online color version of this article differentiates sites taken in a time series from the Lake Helen (orange, green, blue, and purple) and Isunngua regions (red). [Color figure can be viewed at wileyonlinelibrary.com]

Table 2. DOC concentration and DOM composition data from 41 sampling locations west of the Greenland Ice Sheet. Component loadings can be found in Supporting Information Table S1 and Fig. S1.

Sample name	Region	Date	DOC (mg L⁻¹)	Abs (m⁻¹)	SUVA₂₅₄ (L mg C⁻¹ m⁻¹)	S_R	Aliphatic compounds (%RA)	Highly unsaturated and phenolic compounds (%RA)	Polyphenolic (%RA)	Condensed aromatics (%RA)	Formulae (#)	%C1	%C2	%C3	%C4	Total fluorescence (R.U.)
GL1	Isunngua[I]	05 Jun 13	13.61	51.57	3.80	0.718	1	46	31	22	15773	46	28	20	6	3.6
GL2	Isunngua[I]	13 Jul 13	32.05	72.69	2.28	0.896	2	75	16	6	13594	34	30	32	5	7.7
GL3	Isunngua[I]	30 Jul 13	29.33	58.18	1.98	0.909	3	80	13	4	14372	33	30	32	5	6.3
GL4	Isunngua	05 Jun 13	18.18	58.48	3.23	0.753	1	63	24	11	16288	42	31	23	4	5.2
GL5	Isunngua	05 Jun 13	18.28	58.93	3.24	0.745	1	56	27	15	14898	42	31	23	4	5.3
GL6	Isunngua	05 Jun 13	17.38	53.15	3.09	0.773	1	60	25	13	16714	43	31	22	4	5.1
GL7	Isunngua	08 Jun 13	14.60	51.74	3.53	0.750	1	55	27	17	13317	43	31	21	4	4.3
GL8	Isunngua	08 Jun 13	18.28	63.70	3.48	0.733	1	55	28	16	13733	44	31	22	4	5.5
GL9	Lake Helen[II]	09 Jun 13	7.60	12.35	1.64	0.892	3	77	14	6	9112	29	31	30	9	1.2
GL10	Lake Helen[II]	12 Jul 13	15.56	25.68	1.66	0.944	3	83	10	3	9927	29	31	33	7	2.5
GL11	Lake Helen[II]	28 Jul 13	17.35	25.54	1.49	0.951	4	84	9	2	9363	28	31	35	7	2.5
GL12	Lake Helen[III]	09 Jun 13	10.03	24.99	2.48	0.824	2	70	18	9	10444	38	32	23	7	2.0
GL13	Lake Helen[III]	12 Jul 13	11.44	20.05	1.74	0.868	2	82	12	4	7778	33	34	28	5	1.8
GL14	Lake Helen[III]	28 Jul 13	14.02	21.94	1.59	0.864	2	86	9	2	8388	35	34	27	4	2.1
GL15	Lake Helen[IV]	09 Jun 13	12.98	28.26	2.17	0.874	2	79	13	5	10506	37	32	25	7	2.4
GL16	Lake Helen[IV]	12 Jul 13	11.81	21.13	1.78	0.898	2	85	10	2	10109	34	35	26	4	1.9
GL17	Lake Helen[IV]	28 Jul 13	12.78	21.94	1.71	0.860	2	81	12	4	8294	35	35	26	4	2.0
GL18	Lake Helen[V]	11 Jun 13	11.99	20.38	1.71	0.919	3	85	9	2	8540	32	32	29	7	1.9
GL19	Lake Helen[V]	12 Jul 13	16.23	27.98	1.73	0.914	2	85	9	3	9049	31	28	34	7	3.9
GL20	Lake Helen[V]	28 Jul 13	21.35	37.93	1.80	0.857	2	85	10	3	11059	36	33	28	4	3.6
GL21	Qorlortoq	22 Jul 13	9.71	13.50	1.38	1.084	2	84	10	3	7059	26	30	35	8	1.2
GL22	Qorlortoq	22 Jul 13	10.08	14.41	1.41	1.027	3	88	7	1	6347	28	31	33	7	1.4
GL23	Qorlortoq	21 Jul 13	10.25	14.54	1.40	1.076	2	84	10	3	7454	28	32	33	7	1.3
GL24	Qorlortoq	21 Jul 13	11.05	15.49	1.39	1.050	2	85	9	3	7320	28	32	33	7	1.4
GL25	Qorlortoq	19 Jul 13	14.10	30.77	2.17	0.819	1	83	11	3	9480	39	34	22	4	3.0
GL26	Qorlortoq	19 Jul 13	16.67	35.61	2.13	0.846	2	81	13	4	12791	37	33	25	4	3.6
GL27	Qorlortoq	20 Jul 13	15.72	21.18	1.37	1.040	2	82	11	4	7949	28	30	35	7	2.2
GL28	Qorlortoq	20 Jul 13	5.96	5.99	0.98	1.288	3	91	5	1	7787	22	27	38	13	0.5
GL29	Qorlortoq	20 Jul 13	5.67	6.84	1.17	1.057	2	86	8	2	6327	27	31	32	10	0.6
GL30	Qorlortoq	21 Jul 13	8.56	12.96	1.49	0.983	2	85	10	3	7504	35	33	27	5	1.0
GL31	Qorlortoq	23 Jul 13	18.70	23.05	1.23	1.101	4	90	5	1	6080	25	30	38	7	2.1
GL32	Nerumaq	30 Jun 13	2.06	4.62	2.21	0.802	2	71	18	8	11592	37	34	20	8	0.4
GL33	Nerumaq	30 Jun 13	2.16	4.80	2.18	0.769	2	77	15	5	11767	38	34	20	8	0.4
GL34	Nerumaq	02 Jul 13	2.17	4.70	2.14	0.772	2	70	18	9	11737	36	33	22	9	0.4
GL35	Nerumaq	01 Jul 13	1.79	3.78	2.03	0.810	2	76	15	7	9171	36	32	21	11	0.3
GL36	Nerumaq	26 Jun 13	3.82	10.38	2.69	0.835	3	63	23	11	17097	39	29	22	10	0.9
GL37	Sisimiut	18 Jun 13	1.02	2.39	2.16	0.778	4	60	22	10	17500	35	25	19	21	0.2
GL38	Sisimiut	23 Jun 13	1.46	3.61	2.35	0.782	2	60	24	13	16042	38	26	18	18	0.3
GL39	Sisimiut	19 Jun 13	1.80	5.47	2.93	0.773	2	58	26	13	13848	42	26	18	14	0.4
GL40	Sisimiut	19 Jun 13	1.99	6.27	3.05	0.756	1	50	30	18	16011	40	26	19	15	0.4
GL41	Sisimiut	19 Jun 13	2.12	6.69	3.06	0.723	1	50	30	19	12850	41	30	18	12	0.4

%C1–%C4, percent of total fluorescence of each PARAFAC analysis component; %RA, percent relative abundance; R.U., Raman units; S_R, spectral ratio. Roman numerals indicate sites sampled in a time series where numerals correspond to red numerals (I), orange (II), green (III), blue (IV), and purple (V) numbers in Figures 2–4 and 6–8.
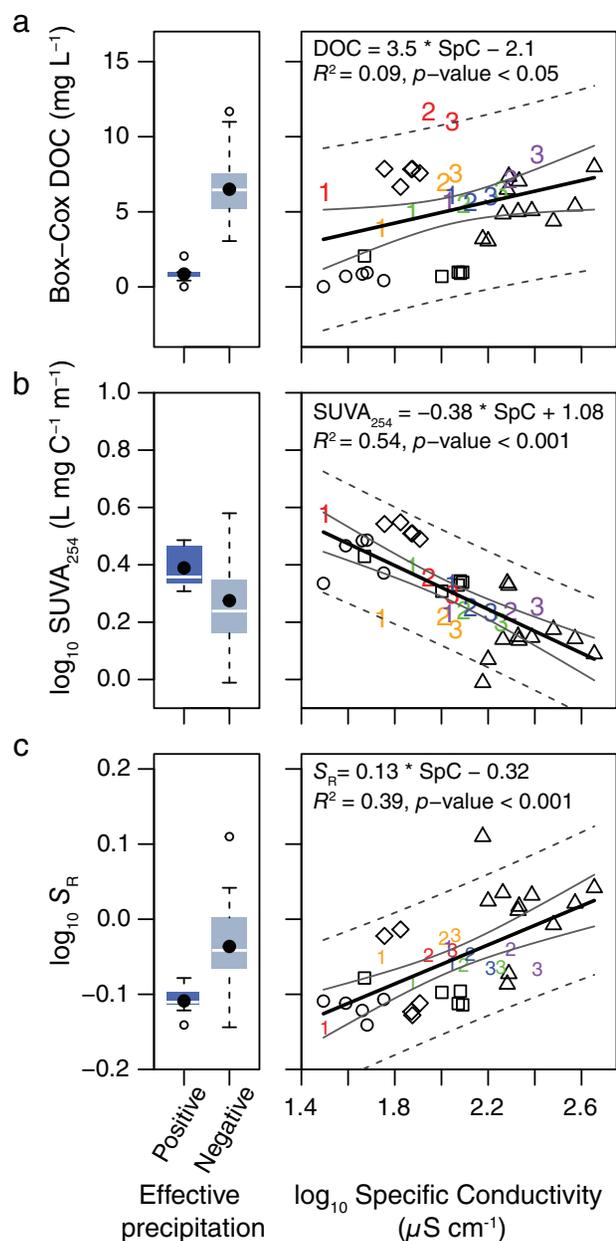
Fig. 3. DOC concentration and optical properties with evaporative state. Panels show differences in (**a**) Box-Cox transformed DOC concentration, (**b**) $\log_{10}$ SUVA$_{254}$, and (**c**) log-transformed S_R at sites with positive and negative precipitation and with increasing $\log_{10}$ SpC. Regression equations are for transformed variables. Mean values in boxplots are indicated by black filled circles and median values are represented by horizontal white lines with the exception of DOC concentration in (**a**) where the box is smaller than the width of the line. All other symbols and lines are as described in Fig. 2. [Color figure can be viewed at wileyonlinelibrary.com]

increased weakly with SpC ($R^2 = 0.09$, $p < 0.05$, Fig. 3a), due to high DOC concentrations observed in the Isunngua region at low SpC. Excluding these sites, DOC concentration increased significantly with SpC in a log-log fashion ($R^2 = 0.46$, $p < 0.001$). SUVA$_{254}$ ranged from 0.98 to 3.80 L mg C^{-1} m^{-1} (2.12 ± 0.73 L mg C^{-1} m^{-1}), and S_R ranged from 0.72 to 1.29

(0.89 ± 0.13; Table 2). Sites with negative effective precipitation exhibited more extreme SUVA$_{254}$ and S_R, despite lower average SUVA$_{254}$ values ($t(29.8) = -2.5$, $p < 0.05$) and higher S_R overall ($t(37.7) = 6.2$, $p < 0.001$). These optical properties were significantly linked to SpC ($p < 0.001$): SUVA$_{254}$ decreased with increasing SpC, whereas S_R increased (Fig. 3b,c).

PARAFAC analysis was used to deconvolute EEMs into four components. Component 1 (C1) was a humic-like component with excitation peaks at 250 and 330 nm and emission at 478 nm, previously identified as photo-reactive (Cory et al. 2007). C2 was characterized as an autochthonous "microbial humic-like" peak (Ex/Em = 250 and 320 nm/410 nm), similar to a component that persists in boreal lakes with long water residence times (Kothawala et al. 2014). Although C3 was characterized as microbial humic-like peak (Ex/Em = 250 and 290 nm/378 nm), it was blue-shifted compared to C2 and had a reduced excitation and broader emission range, characteristics of CDOM photo-degradation (Stedmon et al. 2007). C4 was considered an autochthonous protein-like peak (Ex/Em: 270/302 nm), similar to the tyrosine-like peak (Fellman et al. 2010). Component loadings are found in Supporting Information Table S1 and Fig. S1. Total fluorescence was positively correlated with DOC concentration ($R^2 = 0.82$, $p < 0.001$). The percent contribution of C1 (%C1) comprised the largest fraction of fluorescence (mean ± SD: 34.8% ± 5.8%; Table 2) and decreased with increasing $\log_{10}$ SpC ($R^2 = 0.38$, $p < 0.001$). Percentages of C2 and C3 (%C2: 30.9% ± 2.5%; %C3: 26.5% ± 6.0%; Table 2) increased with increasing $\log_{10}$ SpC (%C2: $R^2 = 0.23$, $p < 0.001$; %C3: $R^2 = 0.45$, $p < 0.001$). However, %C3 was higher in sites with positive effective precipitation, whereas %C2 was not significantly different. %C4 (mean: 7.7% ± 4.0%; Table 2) was higher in sites with positive effective precipitation ($p < 0.001$), but the decrease in %C4 with $\log_{10}$ SpC was not significant after correcting for heteroscedasticity due to high variance at sites with low SpC.

Molecular composition from ultrahigh resolution mass spectrometry

The molecular composition of DOM in aquatic ecosystems in western Greenland, as determined by FT-ICR MS, was consistent with the optical properties. For example, polycyclic and condensed aromatic compounds as well as polyphenolic compounds were positively correlated to SUVA$_{254}$ (polycyclic and condensed aromatics: $R^2 = 0.85$, $p < 0.001$; polyphenolic compounds: $R^2 = 0.89$, $p < 0.001$). Aliphatic compounds and highly unsaturated and phenolic compounds were positively related to S_R (aliphatic compounds: $R^2 = 0.28$, $p < 0.001$; highly unsaturated and phenolic compounds: $R^2 = 0.60$, $p < 0.001$).

The number of molecular formulae totaled 28,824, with 4039 molecular formulae common to all samples. Common formulae (molecular formulae present in all samples) were dominated by molecular formulae containing only the elements C, H, and O (2783; 69%), whereas nonubiquitous formulae were dominated by heteroatomic assignments

(70%). Common CHON formulae were the second most abundant (867), followed by CHOS (389). Common formulae were dominated by highly unsaturated and phenolic compounds (3106), then polyphenolic (547), aliphatic (184), and condensed aromatic formulae (168).

The number of molecular formulae was higher in areas where effective precipitation was positive ($13,760 \pm 2790$) than negative ($10,240 \pm 3170$; $p < 0.001$). The number of formulae decreased exponentially with increasing SpC reaching an asymptote at ~ 7000 molecular formulae ($R^2 = 0.62$, $p < 0.01$ for all terms), that is, the molecular richness decreased with SpC. The relative abundances of polyphenolic compounds and polycyclic and condensed aromatic compounds were elevated in sites with positive effective precipitation ($p < 0.01$ for both comparisons) and decreased exponentially with increasing SpC (Fig. 4a,b). Highly unsaturated and phenolic compounds were elevated in sites with negative effective precipitation, increased exponentially with SpC, and reached an asymptote at ~ 88% relative abundance (Fig. 4c). Aliphatic compounds represent a small fraction of the total relative abundance ($\leq 4\%$) and did not vary significantly with SpC (Table 2). The percent of formulae in the CHO ($55\% \pm 7\%$), CHON ($32\% \pm 6\%$), CHOS ($12\% \pm 2\%$), and CHONS ($1\% \pm 1\%$) classes did not differ significantly between positive and negative effective precipitation. Yet, all classes changed significantly with $\log_{10}$ SpC: CHO and CHOS increased with $\log_{10}$ SpC (CHO: $R^2 = 0.55$, $p < 0.001$; CHOS: $R^2 = 0.29$, $p < 0.01$) and CHON and CHONS decreased with $\log_{10}$ SpC (CHON: $R^2 = 0.65$, $p < 0.001$; CHONS: $R^2 = 0.53$, $p < 0.001$).

A similar pattern can be observed when assessing the relationships between SpC and the relative abundance of individual molecular formula using Spearman rank correlation (Fig. 5). Molecular formulae negatively associated with SpC were predominantly aromatic compounds. Highly unsaturated and phenolic compounds with O/C > 0.5 were positively associated with SpC. N-containing condensed aromatic compounds and polyphenolics were negatively associated with SpC, and few N-containing compounds were positively associated with SpC (Fig. 5b). S-containing compounds were similar to CHO formulae where polyphenolic and condensed aromatic compounds were negatively associated with SpC, and highly unsaturated and phenolic compounds with O/C > 0.5 were positively associated with SpC (Fig. 5c).

Changes in DOC concentration and DOM composition over time

At sites sampled in a time series, $\log_{10}$ DOC concentration increased ($R^2 = 0.29$, $p < 0.05$; Fig. 6a). After correcting for statistically higher variance in $SUVA_{254}$ among sites at the beginning of the season (Breusch-Pagan test for heteroscedasticity, $p < 0.05$), $SUVA_{254}$ decreased significantly over time ($R^2 = 0.22$, $p < 0.05$; Fig. 6b). In contrast, S_R did not change significantly over the summer (Fig. 6c). No change in %C1–3 was observed over the

summer; only %C4 decreased over the summer ($R^2 = 0.45$, $p < 0.01$; Table 2).

Variance in contributions from different compound categories at sites taken in a time series was greatest early in the summer (Fig. 7). Decreases in relative abundances of polycyclic and condensed aromatic compounds ($R^2 = 0.32$, $p < 0.05$) and in polyphenolic compounds ($R^2 = 0.29$, $p < 0.05$) over time were significant after correcting for heteroscedasticity (Fig. 7a,b).
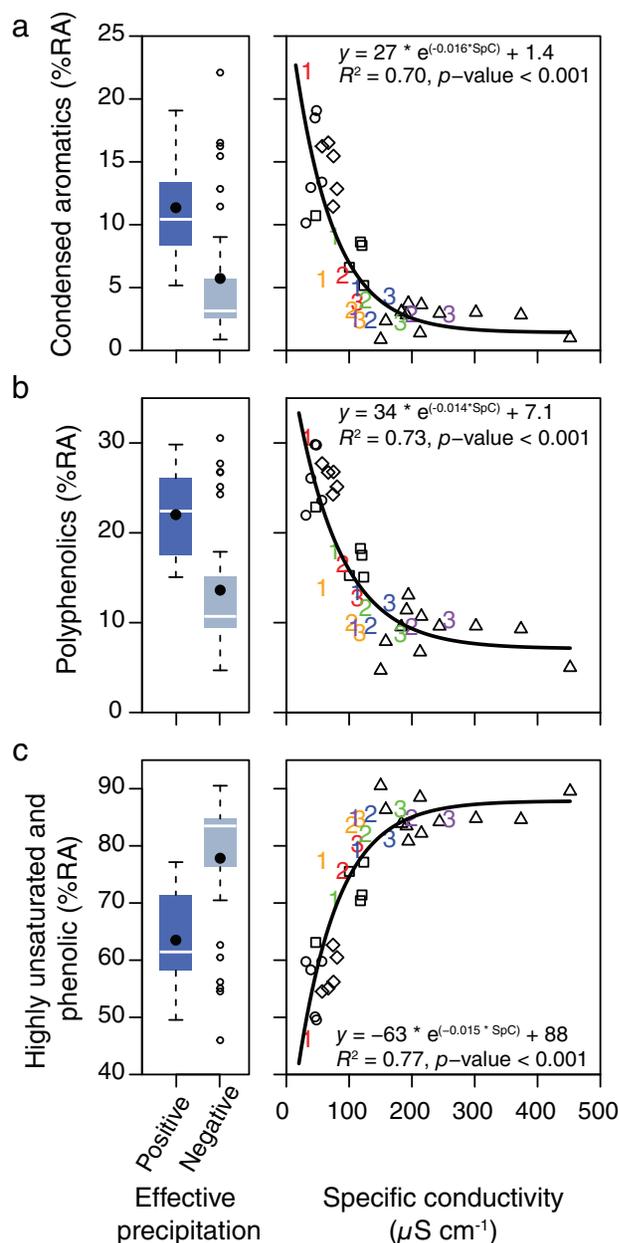
Fig. 4. Changes in compound categories relative to evaporative state. Panels show differences in (**a**) polycyclic and condensed aromatic compounds, (**b**) polyphenolic compounds, and (**c**) highly unsaturated and phenolic compounds with effective precipitation and SpC. Symbols and lines are as described for Figs. 2, 3. [Color figure can be viewed at wileyonlinelibrary.com]
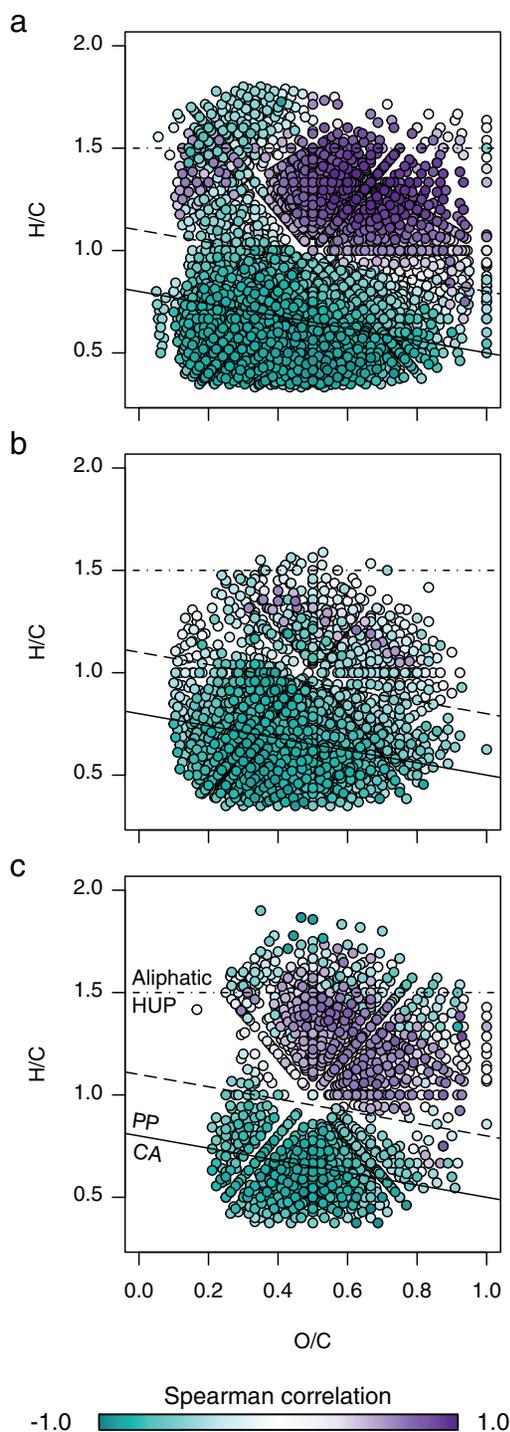
Fig. 5. Van Krevelen diagram showing the associations between individual molecular formula and SpC. Significant (false-discovery rate adjusted *p* < 0.05) Spearman rank correlation coefficients between SpC and (**a**) molecular formula containing only C, H, and O, (**b**) those containing N and (**c**) those containing S. Axes are the molar ratios of O/C and H/C for each molecular formula. Color scale indicates the strength and direction of the Spearman correlation, either negative (turquoise) or positive (purple). Lines approximately delineate compound groups. CA, condensed aromatic compounds; HUP, highly unsaturated and phenolic compounds; PP, polyphenolic compounds.
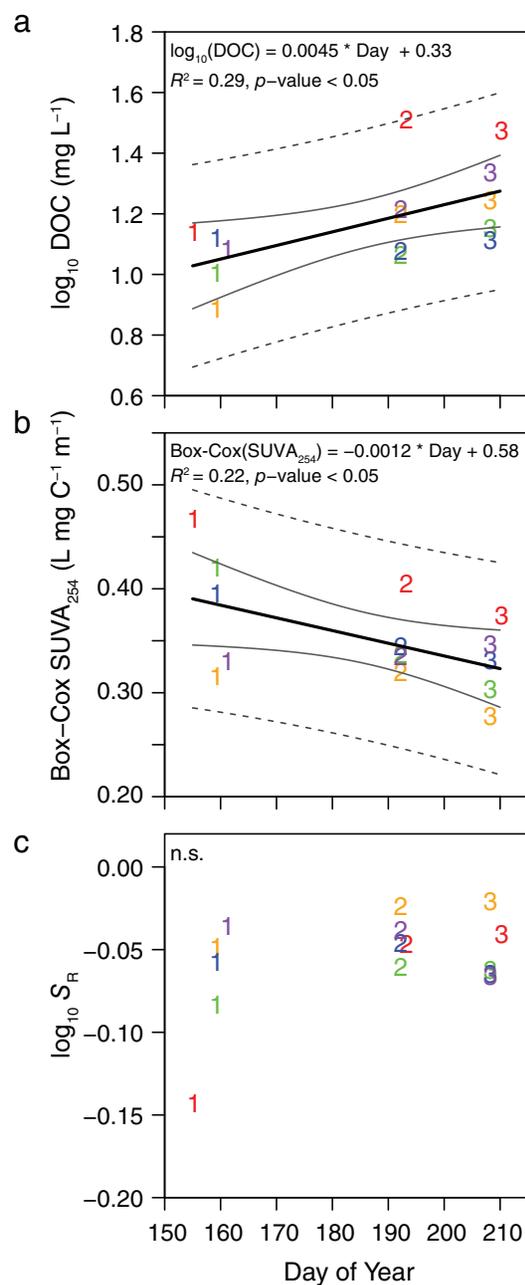
Fig. 6. Changes in DOC concentration and optical properties over time. Panels show differences in (a) log10 DOC concentration, (b) Box-Cox transformed SUVA254, and (c) log10 SR over time. All sites sampled in a time series have negative effective precipitation. Black lines represents regression lines, and the solid gray and dashed gray lines represent the 95% confidence and prediction intervals, respectively. The online version shows colors that indicate sites taken in a time series from the Lake Helen (orange, green, blue, and purple) and Isunngua (red) regions. [Color figure can be viewed at wileyonlinelibrary.com]

Although highly unsaturated and phenolic compounds increased over the season, the Box-Cox transformation was not successful in eliminating heteroscedasticity (Fig. 7c). The
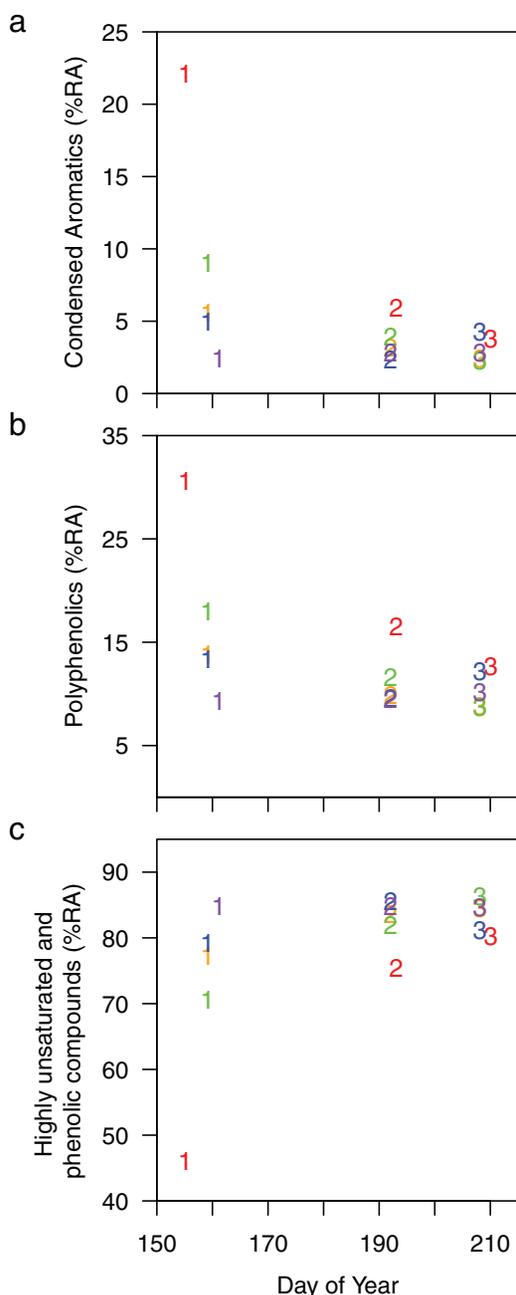
Fig. 7. The percent relative abundance of (**a**) condensed aromatics, (**b**) polyphenolic compounds, and (**c**) highly unsaturated and phenolic compounds over time. All relationships exhibited heteroscedasticity using the Breusch-Pagan test, with higher variance earlier in the season. The decrease in (**a**) and (**b**) was significant ($p < 0.05$) after correcting for heteroscedasticity. The Box-Cox transformation of (**c**) was unsuccessful in eliminating heteroscedasticity. Symbols are as described for Fig. 6. [Color figure can be viewed at wileyonlinelibrary.com]

Fig. 8. Nonmetric multidimensional scaling of dissolved organic molecules from 41 aquatic systems west of the Greenland Ice Sheet. The NMDS (stress = 0.04, $k = 3$) shows (**a**) relationships between sites based on (**b**) DOM composition derived from FT-ICR MS, with optical and environmental data fit to the ordination over 999 permutations. Sisimiut (circles) and Nerumaq (squares) regions have positive effective precipitation, whereas Qorlortoq (triangles), Lake Helen (numbers), and Isunngua (numbers and diamonds) regions have negative effective precipitation. Numbers indicate sites that were sampled in a time series. HUPs (% RA), highly unsaturated and phenolic compounds (% relative abundance). In the online version, color is used to distinguish between sites sampled in a time series as in Fig. 6. [Color figure can be viewed at wileyonlinelibrary.com]

Multivariate relationships

NMDS using Bray-Curtis dissimilarity showed a separation along the first dimension between sites with high SUVA$_{254}$ values and sites with high SpC and enriched water isotopes

relative abundance of aliphatic compounds did not change appreciably over time and neither did the relative contributions of CHO, CHON, CHOS, and CHONS molecular formulae.
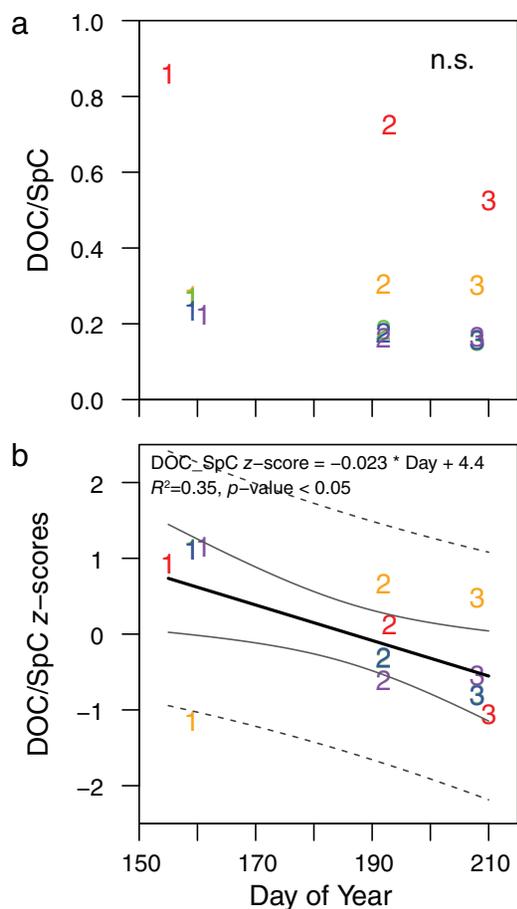
Fig. 9. Relative evapoconcentration of DOC concentration and SpC over time as (**a**) original values and (**b**) *z*-scores. [Color figure can be viewed at wileyonlinelibrary.com]

(stress = 0.04, *k* = 3; NMDS1; Fig. 8). The NMDS illustrated how sites were related (Fig. 8a) based on the FT-ICR MS derived molecular composition (Fig. 8b) and exhibited a nonmetric fit between observed dissimilarity and ordination distance with an R^2 = 0.99. The decrease in condensed aromatic and polyphenolic compounds coincided with a decrease in %C1 and an increase in the relative abundance of aliphatic compounds and highly unsaturated and phenolic compounds (Fig. 8). DOC concentration separated perpendicular to $SUVA_{254}$ and SpC, on the second dimension (NMDS2). The third dimension, while necessary for achieving convergence with adequately low stress, did not reveal unique patterns.

Discussion

DOM composition across an effective precipitation gradient

Aquatic ecosystems in the deglaciated landscape of western Greenland have highly variable DOC concentrations and DOM compositional characteristics, both across and within regions (Figs. 3–5). Lakes in regions with negative effective precipitation have long water residence times due to limited precipitation and

runoff and elevated SpC caused by evaporative concentration (Anderson and Stedmon 2007). Although SpC is not a control on DOM composition, it reflects the balance between inputs and evapoconcentration of solutes, and thus can be related to the inputs of and processing undergone by DOM in these systems.

Long water residence times and extensive daylight hours in the summer allow more time for in situ DOM production and photobleaching to occur. Polyphenolic and condensed aromatic compounds have been linked to terrestrial sources (Kellerman et al. 2018). These highly aromatic, and thus, photoreactive dissolved organic molecules (e.g., Stubbins et al. 2010) would be expected to decrease in number and relative abundance as SpC increases, thereby increasing the relative abundance of less conjugated groups like the highly unsaturated and phenolic compounds. Additionally, extended water residence times allow for autochthonous production and microbial degradation of DOM, leading to increases in molecular richness and the relative abundances of aliphatic and N-containing compounds (Osterholz et al. 2016). Molecular richness in these systems decreased with increasing SpC, and while median values were similar, the interquartile range was 3–4 times wider to those previously reported in a wide range of lakes and rivers (Kellerman et al. 2018). In systems with limited allochthonous inputs, microbial communities have been hypothesized to support the observed molecular diversity (Noriega-Ortega et al. 2019). However, studies in freshwater systems have shown a decreasing molecular diversity with increasing time in the hydrologic network (Kellerman et al. 2014; Mosher et al. 2015), suggesting the variability of inputs in freshwater systems may control chemodiversity. As the variability of DOM inputs decreases with hydrologic disconnection, molecular diversity also decreases (Table 2). Because negative effective precipitation results in both high SpC through evapoconcentration and compositional changes due to extended water residence times, SpC explains $\geq$ 70% of the variability in the condensed aromatic, polyphenolic and highly unsaturated and phenolic compound classes. These three classes account for > 90% of the relative abundance of the molecular formulae in this data set (Table 2; Fig. 4).

Across the effective precipitation gradient, DOC concentration increased weakly with SpC due to high variability at low SpC (Fig. 3a), likely due to differing lateral inputs of meltwater in the spring, amounts of vegetation within the catchment, and fringing wetlands. The low DOC concentrations and SpC where effective precipitation is positive are typical of Arctic lakes (Seekell et al. 2015; Osburn et al. 2017). Elevated DOC concentrations are generally observed during spring freshet (Raymond et al. 2007; Spencer et al. 2009; Stedmon et al. 2011) and in areas with high mean annual precipitation (Kellerman et al. 2014). Runoff increases with precipitation and snowmelt, and transports allochthonous DOM and other nutrients into aquatic ecosystems (Spencer et al. 2008; Raymond et al. 2016). Precipitation and snowmelt may also recharge wetlands, which export high concentrations of aromatic DOM (Aitkenhead and McDowell 2000; Spencer et al. 2013). Evaporation alone would increase DOC

concentration concurrent with SpC, as evaporation in arid regions acts as a perennial control of solute concentrations in the absence of flooding (Wiklund et al. 2012; Bianchi et al. 2017). The extent to which evaporation can influence DOC concentration depends on the water residence time (Jones et al. 2018). Short water residence times are dominated by hydrologic flushing such as at the sites with positive effective precipitation. Alternatively, factors associated with lengthened water residence times, such as length of UV exposure and length of time for DOM production and processing, could outweigh the effects of evaporation on both DOC concentration and DOM composition. The DOC concentrations in the sites sampled here were below the median value observed in this region previously (Osburn et al. 2017), suggesting that the secondary effects of evaporative concentration in the Greenland watersheds with negative effective precipitation as shown by the increased relative abundance of highly unsaturated and phenolic compounds (Fig. 4c) may be exacerbated further in closed basin systems.

Sources of DOM

DOM in aquatic systems in semiarid catchments is often attributed to autochthonous sources (Anderson and Stedmon 2007; Osburn et al. 2011, 2017; Bogard et al. 2019). N-containing compounds that were positively associated with SpC in our study may be produced in situ, despite being less saturated than aminosugars (Rivas-Ubach et al. 2018). Alternatively, they may result from incomplete photochemical degradation of N-containing polyphenolic compounds (Stubbins et al. 2010; Stubbins and Dittmar 2015). Few N-containing compounds were positively associated with SpC (Fig. 5b), consistent with the high C/N ratios previously attributed to allochthonous DOM sources in semiarid lakes in Alberta (Curtis and Adams 1995). Aliphatic, N-containing, and S-containing compounds detected by FT-ICR MS have been linked to chlorophyll *a* (Osterholz et al. 2016), a proxy for primary production. Aliphatic compounds have also been found to be particularly susceptible to microbial degradation, although microbial degradation has been linked to the loss of a variety of molecular formulae (D'Andrilli et al. 2015; Spencer et al. 2015; Mostovaya et al. 2017). The relative abundance comprised by aliphatic compounds in the current study was lower than previously observed in lakes and rivers (Wagner et al. 2015; Kellerman et al. 2018). While aliphatic compounds exhibit a positive loading on the first axis of the principal component analysis (Fig. 8), they did not change significantly with SpC or over time, suggesting there is a small (2% ± 1% relative abundance) homeostatic pool of aliphatic compounds microbially cycled in these systems.

The fraction of N- and S-containing molecular formulae were also similar to or lower than previously observed in lakes and rivers (Spencer et al. 2014; Wagner et al. 2015; Kellerman et al. 2018), suggesting these sites are not anomalous in heteroatomic composition. In this study, N-containing compounds associated with SpC (n = 3895) were largely polyphenolic (45%) or condensed aromatic (23%) molecular formulae that negatively

covary with SpC (Fig. 5b). Many S-containing compounds associated with SpC (n = 1925) were polyphenolic (22%) and condensed aromatic (17%) molecular formulae that negatively covary with SpC. However, highly unsaturated and phenolic S-containing compounds associated with SpC (50%, n = 955) were split between being negatively (53%) and positively (47%) correlated with SpC (Fig. 5). S-containing compounds have been linked to autochthonous production (Osterholz et al. 2016), likely dominated by littoral macrophytes and benthic autotrophs in these systems (Osburn et al. 2017). The dominance of heteroatomic elements in nonubiquitous molecular formulae has been attributed to anthropogenic inputs (Wagner et al. 2015), but N- and S-containing molecular formulae in polyphenolic and condensed aromatic categories is typical of wetland inputs (Sleighter et al. 2014). The negative relationship of aromatic formulae with SpC suggests decreased inputs and increased photodegradation with heightened evaporative state. While a decrease in relative abundance may reflect an increase in the relative abundance of other peaks, the number of N- and S-containing formulae and the total number of molecular formulae decreased with increasing SpC.

Contributions of condensed aromatic and polyphenolic compounds are similar to those previously observed in lakes and rivers; however, the median contribution of highly unsaturated and phenolic compounds in sites with negative effective precipitation falls between that observed in lakes and the ocean (Stubbins and Dittmar 2015; Kellerman et al. 2018). DOC concentrations in sites with negative effective precipitation were 1–2 orders of magnitude higher than that observed in the ocean, suggesting a concentration of DOM resistant to further photodegradation. The concentration of photoproducts from polyphenolic and condensed aromatic degradation was further supported by the fluorescence data. The photosensitive humic-like fluorescence of %C1 decreased with increasing SpC (Fig. 8), which suggests that %C1 was photodegraded with increased residence time (Cory et al. 2007; Helms et al. 2013, 2014; Lu et al. 2013). %C2 and %C3, the fractions of which increased with DOC concentration, were either by-products of C1 photodegradation (Fellman et al. 2010; Kothawala et al. 2014) or produced in situ. %C4, the protein-like component, was negatively associated with DOC concentration and was highest at coastal sites, where DOC concentration and total fluorescence were low (Fig. 8). %C2 and %C3 were low near the coast (positive effective precipitation), suggesting limited photodegradation consistent with the high cloud cover and dense fog banks characteristic of the coastal environment (Anderson and Stedmon 2007), and resulted in a higher %C4 despite minimal DOC concentration (Fig. 8). Furthermore, %C4 was the only fluorescence component that decreased significantly over the summer, whereas the decrease in %C1 was not significant after correcting for heteroscedasticity. High %C4 at the coast and the decrease in %C4 over the summer may reflect patterns in recent microbial and algal production. However, protein-like fluorescence is a result of the indolic and phenolic structures within tryptophan and tyrosine, respectively, thus

nonproteinaceous molecules containing these moieties can produce similar fluorescence spectra (Maie et al. 2007; Wünsch et al. 2015). For example, protein-like fluorescence has previously been related to lignin phenol concentrations (Hernes et al. 2009), so decreases in %C4 may reflect lower lignin concentrations in sites with high SpC and throughout the summer. Therefore, from positive to negative effective precipitation, DOM composition exhibits decreases in aromaticity and N-containing compounds, which suggests allochthonous DOM is transported into these systems and extensively photodegraded.

Decoupling of DOC concentration and DOM composition

The relationships between SpC and DOM composition at sites sampled over time suggest DOM composition changes due to photodegradation over a single summer. The magnitude of these changes depends on composition at the beginning of the summer, which is controlled by the extent of hydrologic connectivity. Allochthonous DOM may be delivered from snowmelt inundated wetlands or seepage through permafrost, which underlays the area (Jørgensen and Andreasen 2007). The overall depletion of δD and $\delta^{18}O$ at the Isunngua sites (Fig. 2a) suggests snowmelt increases hydrologic connectivity and recharges fringing wetlands (Wolfe et al. 2007). This connection delivers allochthonous DOC, which provides new substrate for photochemical degradation and masks the perennial effects of negative effective precipitation. As the season progresses, however, SpC increases (Fig. 2c) suggesting evapoconcentration, photochemical degradation, and photo-enhanced biodegradation likely control DOC concentration and DOM composition. These changes are similar to previous findings where aquatic ecosystems took weeks to return to prefreshet conditions, but several years to regain the characteristics of a system reflecting evaporative concentrative conditions (Wiklund et al. 2012). Although DOM composition exhibited high initial variability, DOM composition converged across sites with increasing SpC (Figs. 3, 4) and throughout time (Figs. 6, 7). Composition converged toward decreased SUVA$_{254}$ values (Fig. 6b), decreased relative abundances of polyphenolic compounds and condensed aromatic compounds, and increased relative abundances of highly unsaturated and phenolic compounds (Fig. 7).

Simultaneous evaporation and incomplete photodegradation (specifically photobleaching) could explain the seasonal shifts in composition without a concurrent decrease in DOC concentration, given the strong decreases in the photochemically active fraction of the DOM pool over the summer (Stubbins et al. 2010, 2017). Photodegradation has been previously suggested as a driver of DOM composition in lakes with long residence times in both boreal (Kellerman et al. 2014) and arid systems (Curtis and Adams 1995), with the main distinction that in boreal lakes, DOM becomes less aromatic and DOC concentrations decrease, whereas in semiarid systems DOM becomes less aromatic but DOC concentrations increase. This loss of aromaticity but increase in DOC concentration in semiarid systems occurs when the rate of evapoconcentration and in situ production exceeds degradation.

Sites with negative effective precipitation increased in both SpC (Fig. 2c; Table 1) and DOC concentration (Fig. 6a; Table 2) over the course of the summer. If evaporation alone was controlling DOC concentration, the DOC concentration to SpC ratio should remain constant; however, this is not the case. The site-specific z-scores of the ratio of DOC concentration to SpC decreased significantly over the summer (Fig. 9; $R^2 = 0.35$, $p < 0.05$). Changes in SpC are conservative, thus the decrease in the ratio through time indicates that DOC was degraded more rapidly than combined in situ production and evapoconcentration because there was a net loss of DOC from the system. Photo-exposure has been found to enhance the bioavailability of DOM (Obernosterer and Benner 2004). Given the concurrent compositional changes of DOM over the summer (Table 2; Figs. 6, 7), combined photodegradation and photo-enhanced biodegradation of DOM appears to be the dominant loss mechanism.

The limited connectivity between aquatic ecosystems and their catchments in semiarid climates results in sporadic transport of allochthonous DOM, which maintains the negative relationship between SUVA$_{254}$ and DOC. This relationship is in contrast with that found in wetter temperate and boreal regions, where aquatic systems are continuously connected to their watersheds, and high DOC concentrations are typically characterized by high SUVA$_{254}$ (Kothawala et al. 2014). However, in this study, DOC concentration and SUVA$_{254}$ are disassociated (Fig. 8; that is, neither positively nor negatively associated). Furthermore, sites sampled in a time series exhibited significant decreases in SUVA$_{254}$, condensed aromatic compounds, and polyphenolic compounds (Figs. 6, 7). These results, along with the temporal decrease in DOC/SpC, suggest there is a pulse of aromatic DOM from snowmelt inundated wetlands early in the season that is then processed out of the system. In addition to wetland inputs, the leaching of aromatic DOM is enhanced during the reinundation of previously dried systems (Bianchi et al. 2017). Thus, lateral inputs from melting snow and thawing permafrost near the ice sheet disrupt typical relationships between DOC concentration and DOM composition found in other landscapes, creating a scenario where sites with negative effective precipitation experience seasonal connection to the landscape before becoming disconnected over the summer. This may be exacerbated by a shallow active layer which keeps water near the soil surface early in the spring and flushes surface organic rich soils and litter layers (Kurylyk et al. 2014), in an area that may otherwise have continuously low hydrologic connectivity based on high levels of evaporation and low runoff (Good et al. 2015).

Implications for C cycling across gradients of effective precipitation

Deglaciated catchments in western Greenland are littered with aquatic systems that have highly variable DOC concentrations and DOM composition. Positive effective precipitation and cloud cover resulted in low DOC concentrations and a low degree of photodegradation near the coast. Inland, runoff from

snowmelt increased hydrologic connectivity of aquatic systems in semiarid environments within their catchments, delivering highly aromatic, photodegradable DOM that countered the secondary effects of negative effective precipitation in the short term. As the summer progressed in areas with negative effective precipitation, a net loss of organic carbon was observed, and evapoconcentration, photodegradation, and potentially photo-enhanced biodegradation dominated as controls on DOC concentration and DOM composition, shifting to a more photo-refractory elemental composition (Stubbins et al. 2010). This relationship suggests that as DOM is photodegraded, what remains is inherently more stable. Although many studies show that DOC concentration and aromaticity are related, either positively in wetter climates (Spencer et al. 2009; Stedmon et al. 2011; Kothawala et al. 2014; Seekell et al. 2015; Mann et al. 2016), or negatively in semi-arid climates (Curtis and Adams 1995; Osburn et al. 2011), they are decoupled across western Greenland. This pattern results from the shift in effective precipitation over a relatively small, but complex hydrologic environment that also encompasses snowmelt fed wetlands and permafrost active layer thaw. Constraining DOC export from deglaciated areas in Greenland is further hampered by rapidly changing hydrology each season and lack of discharge data. Additionally, as glaciers retreat, the associated katabatic winds will also retreat, potentially shifting the boundary between positive and negative effective precipitation inland (Scribner et al. 2015). Finally, this study highlights the subtleties of predicting how retreat of the Greenland Ice Sheet will impact regional C dynamics due to difficulties in assessing how and where shifting hydrologic connectivity may increase wetland development and associated DOC and CDOM export.

References

Aiken, G. R., H. Hsu-Kim, and J. N. Ryan. 2011. Influence of dissolved organic matter on the environmental fate of metals, nanoparticles, and colloids. Environ. Sci. Technol. **45**: 3196–3201. doi:10.1021/es103992s

Aitkenhead, J. A., and W. H. McDowell. 2000. Soil C:N ratio as a predictor of annual riverine DOC flux at local and global scales. Global Biogeochem. Cycles **14**: 127–138. doi:10.1029/1999GB900083

Anderson, N. J., R. Harriman, D. B. Ryves, and S. T. Patrick. 2001. Dominant factors controlling variability in the ionic composition of West Greenland Lakes. Arct. Antarct. Alp. Res. **33**: 418–425. doi:10.2307/1552551

Anderson, N. J., and C. A. Stedmon. 2007. The effect of evapoconcentration on dissolved organic carbon concentration and quality in lakes of SW Greenland. Freshw. Biol. **52**: 280–289. doi:10.1111/j.1365-2427.2006.01688.x

Ask, J., J. Karlsson, L. Persson, P. Ask, P. Bystrom, and M. Jansson. 2009. Terrestrial organic matter and light penetration: Effects on bacterial and primary production in lakes.

Limnol. Oceanogr. **54**: 2034–2040. doi:10.4319/lo.2009.54.6.2034

Battin, T. J., S. Luyssaert, L. A. Kaplan, A. K. Aufdenkampe, A. Richter, and L. J. Tranvik. 2009. The boundless carbon cycle. Nat. Geosci. **2**: 598–600. doi:10.1038/ngeo618

Benjamini, Y., and Y. Hochberg. 1995. Controlling the false discovery rate—a practical and powerful approach to multiple testing. J. R. Stat. Soc. B **57**: 289–300. Available from www.jstor.org/stable/2346101

Bianchi, T. S., and others. 2017. The experimental flow to the Colorado River Delta: Effects on carbon cycling. J. Geophys. Res. Biogeosci. **122**: 607–627. doi:10.1002/2016JG003555

Bogard, M. J., and others. 2019. Negligible cycling of terrestrial carbon in many lakes of the arid circumpolar landscape. Nat. Geosci. **12**: 180–185. doi:10.1038/s41561-019-0299-5

Brooks, J. R., J. J. Gibson, S. J. Birks, M. H. Weber, K. D. Rodecap, and J. L. Stoddard. 2014. Stable isotope estimates of evaporation : Inflow and water residence time for lakes across the United States as a tool for national lake water quality assessments. Limnol. Oceanogr. **59**: 2150–2165. doi:10.4319/lo.2014.59.6.2150

Cory, R. M., D. M. McKnight, Y. P. Chin, P. Miller, and C. L. Jaros. 2007. Chemical characteristics of fulvic acids from Arctic surface waters: Microbial contributions and photochemical transformations. J. Geophys. Res. Biogeosci. **112**: G04S51. doi:10.1029/2006JG000343

Craig, H. 1961. Isotopic variations in meteoric waters. Science **133**: 1702–1703. doi:10.1126/science.133.3465.1702

Curtis, P. J., and H. E. Adams. 1995. Dissolved organic matter quantity and quality from freshwater and saltwater lakes in east-central Alberta. Biogeochemistry **30**: 59–76. doi:10.1007/BF02181040

D'Andrilli, J., W. T. Cooper, C. M. Foreman, and A. G. Marshall. 2015. An ultrahigh-resolution mass spectrometry index to estimate natural organic matter lability. Rapid Commun. Mass Spectrom. **29**: 2385–2401. doi:10.1002/rcm.7400

Dittmar, T., B. Koch, N. Hertkorn, and G. Kattner. 2008. A simple and efficient method for the solid-phase extraction of dissolved organic matter (SPE-DOM) from seawater. Limnol. Oceanogr.: Methods **6**: 230–235. doi:10.4319/lom.2008.6.230

Fellman, J. B., E. Hood, and R. G. M. Spencer. 2010. Fluorescence spectroscopy opens new windows into dissolved organic matter dynamics in freshwater ecosystems: A review. Limnol. Oceanogr. **55**: 2452–2462. doi:10.4319/lo.2010.55.6.2452

Findlay, S., and R. L. Sinsabaugh [eds.]. 2003. Aquatic ecosystems: Interactivity of dissolved organic matter. Elsevier.

Gibson, J. J., S. J. Birks, and T. W. D. Edwards. 2008. Global prediction of δA and $\delta^2 H$-$\delta^{18}O$ evaporation slopes for lakes and soil water accounting for seasonality. Global Biogeochem. Cycles **22**: GB2031. doi:10.1093/pch/13.8.666

Gonsior, M., B. M. Peake, W. T. Cooper, D. Podgorski, J. D'Andrilli, and W. J. Cooper. 2009. Photochemically induced changes in dissolved organic matter identified by ultrahigh resolution Fourier transform ion cyclotron resonance mass spectrometry. Environ. Sci. Technol. **43**: 698–703. doi:10.1021/es8022804

Good, S. P., D. Noone, and G. Bowen. 2015. Hydrologic connectivity constrains partitioning of global terrestrial water fluxes. Science **349**: 175–177. doi:10.1126/science.aaa5931

Guo, L. D., C. H. Coleman, and P. H. Santschi. 1994. The distribution of colloidal and dissolved organic-carbon in the Gulf-of-Mexico. Mar. Chem. **45**: 105–119. doi:10.1016/0304-4203(94)90095-7

Harrell, F. E. 2016. Hmisc: Harrell miscellaneous. R package version 3.17-2.

Hasholt, B., and H. Søgaard. 1978. Et Forsøg På En Klimatisk-Hydrologisk Regionsinddeling Af Holsteinsborg Kommune (Sisimiut). Geografisk Tidsskrift **77**: 72–92. doi:10.1080/00167223.1978.10649095

Helms, J. R., A. Stubbins, J. D. Ritchie, E. C. Minor, D. J. Kieber, and K. Mopper. 2008. Absorption spectral slopes and slope ratios as indicators of molecular weight, source, and photobleaching of chromophoric dissolved organic matter. Limnol. Oceanogr. **53**: 955–969. doi:10.4319/lo.2008.53.3.0955

Helms, J. R., A. Stubbins, E. M. Perdue, N. W. Green, H. Chen, and K. Mopper. 2013. Photochemical bleaching of oceanic dissolved organic matter and its effect on absorption spectral slope and fluorescence. Mar. Chem. **155**: 81–91. doi:10.1016/j.marchem.2013.05.015

Helms, J. R., and others. 2014. Loss of optical and molecular indicators of terrigenous dissolved organic matter during long-term photobleaching. Aquat. Sci. **76**: 353–373. doi:10.1007/s00027-014-0340-0

Hernes, P. J., B. A. Bergamaschi, R. S. Eckard, and R. G. M. Spencer. 2009. Fluorescence-based proxies for lignin in freshwater dissolved organic matter. J. Geophys. Res. **114**: G00F03. doi:10.1029/2009JG000938

Hertkorn, N., and others. 2007. High-precision frequency measurements: Indispensable tools at the core of the molecular-level analysis of complex systems. Anal. Bioanal. Chem. **389**: 1311–1327. doi:10.1007/s00216-007-1577-4

Jones, S. E., J. A. Zwart, P. T. Kelly, and C. T. Solomon. 2018. Hydrologic setting constrains lake heterotrophy and terrestrial carbon fate. Limnol. Oceanogr.: Lett. **3**: 256–264. doi:10.1002/lol2.10054

Jørgensen, A. S., and F. Andreasen. 2007. Mapping of permafrost surface using ground-penetrating radar at Kangerlussuaq Airport, western Greenland. Cold Reg. Sci. Technol. **48**: 64–72. doi:10.1016/j.coldregions.2006.10.007

Kaiser, N. K., J. P. Quinn, G. T. Blakney, C. L. Hendrickson, and A. G. Marshall. 2011. A Novel 9.4 Tesla FTICR Mass Spectrometer with Improved Sensitivity, Mass Resolution, and Mass Range. J. Am. Soc. Mass Spectrom. **22**: 1343–1351. doi:10.1007/s13361-011-0141-9

Kellerman, A. M., T. Dittmar, D. N. Kothawala, and L. J. Tranvik. 2014. Chemodiversity of dissolved organic matter in lakes driven by climate and hydrology. Nat. Commun. **5**: 3804. doi:10.1038/ncomms4804

Kellerman, A. M., D. N. Kothawala, T. Dittmar, and L. J. Tranvik. 2015. Persistence of dissolved organic matter in lakes related to its molecular characteristics. Nat. Geosci. **8**: 454–457. doi:10.1038/ngeo2440

Kellerman, A. M., F. Guillemette, D. C. Podgorski, G. R. Aiken, K. D. Butler, and R. G. M. Spencer. 2018. Unifying concepts linking dissolved organic matter composition to persistence in aquatic ecosystems. Environ. Sci. Technol. **52**: 2538–2548. doi:10.1021/acs.est.7b05513

Koch, B. P., and T. Dittmar. 2006. From mass to structure: An aromaticity index for high-resolution mass data of natural organic matter. Rapid Commun. Mass Spectrom. **20**: 926–932. doi:10.1002/rcm.2386

Koch, B. P., T. Dittmar, M. Witt, and G. Kattner. 2007. Fundamentals of molecular formula assignment to ultrahigh resolution mass data of natural organic matter. Anal. Chem. **79**: 1758–1763. doi:10.1021/ac061949s

Koch, B. P., and T. Dittmar. 2016. From mass to structure: An aromaticity index for high-resolution mass data of natural organic matter. Rapid Commun. Mass Spectrom. **30**: 250–250. doi:10.1002/rcm.7433

Kothawala, D. N., C. A. Stedmon, R. A. Muller, G. A. Weyhenmeyer, S. J. Kohler, and L. J. Tranvik. 2014. Controls of dissolved organic matter quality: Evidence from a large-scale boreal lake survey. Glob. Chang. Biol. **20**: 1101–1114. doi:10.1111/gcb.12488

Kurylyk, B. L., K. T. B. Macquarrie, and J. M. Mckenzie. 2014. Climate change impacts on groundwater and soil temperatures in cold and temperate regions: Implications, mathematical theory, and emerging simulation tools. Earth Sci. Rev. **138**: 313–334. doi:10.1016/j.earscirev.2014.06.006

Leng, M. J., and N. J. Anderson. 2003. Isotopic variation in modern lake waters from western Greenland. Holocene **13**: 605–611. doi:10.1191/0959683603hl620rr

Lu, Y., J. E. Bauer, E. A. Canuel, Y. Yamashita, R. M. Chambers, and R. Jaffe. 2013. Photochemical and microbial alteration of dissolved organic matter in temperate headwater streams associated with different land use. J. Geophys. Res. **118**: 566–580. doi:10.1002/jgrg.20048

Maie, N., N. M. Scully, O. Pisani, and R. Jaffe. 2007. Composition of a protein-like fluorophore of dissolved organic matter in coastal wetland and estuarine ecosystems. Water Res. **41**: 563–570. doi:10.1016/j.watres.2006.11.006

Mann, P. J., and others. 2012. Controls on the composition and lability of dissolved organic matter in Siberia's Kolyma River basin. J. Geophys. Res. Biogeosci. **117**: G01028. doi:10.1029/2011JG001798

Mann, P. J., and others. 2016. Pan-Arctic trends in terrestrial dissolved organic matter from optical measurements. Front. Earth Sci. **4**: 25. doi:10.3389/feart.2016.00025

Massicotte, P., E. Asmala, C. Stedmon, and S. Markager. 2017. Global distribution of dissolved organic matter along the aquatic continuum: Across rivers, lakes and oceans. Sci. Total Environ. **609**: 180–191. doi:10.1016/j.scitotenv.2017.07.076

McClelland, J. W., and others. 2016. Particulate organic carbon and nitrogen export from major Arctic rivers. Global Biogeochem. Cycles **30**: 629–643. doi:10.1002/2015GB005351

McKnight, D. M., E. W. Boyer, P. K. Westerhoff, P. T. Doran, T. Kulbe, and D. T. Andersen. 2001. Spectrofluorometric characterization of dissolved organic matter for indication of precursor organic material and aromaticity. Limnol. Oceanogr. **46**: 38–48. doi:10.4319/lo.2001.46.1.0038

Molot, L. A., and others. 2004. Risk analysis of dissolved organic matter-mediated ultraviolet B exposure in Canadian inland waters. Can. J. Fish. Aquat. Sci. **61**: 2511–2521. doi:10.1139/f04-165

Mosher, J. J., L. A. Kaplan, D. C. Podgorski, A. M. Mckenna, and A. G. Marshall. 2015. Longitudinal shifts in dissolved organic matter chemogeography and chemodiversity within headwater streams: A river continuum reprise. Biogeochemistry. **124**: 371–385. doi:10.1007/s10533-015-0103-6

Mostovaya, A., J. A. Hawkes, T. Dittmar, and L. J. Tranvik. 2017. Molecular determinants of dissolved organic matter reactivity in lake water. Front. Earth Sci. **5**: 106. doi:10.3389/feart.2017.00106

Murphy, K. R., C. A. Stedmon, D. Graeber, and R. Bro. 2013. Fluorescence spectroscopy and multi-way techniques. PARAFAC. Anal. Methods **5**: 6557–6566. doi:10.1039/c3ay41160e

Noriega-Ortega, B. E., G. Wienhausen, A. Mentges, T. Dittmar, M. Simon, and J. Niggemann. 2019. Does the chemodiversity of bacterial exometabolomes sustain the chemodiversity of marine dissolved organic matter? Front. Microbiol. **10**: 215.

Obernosterer, I., and R. Benner. 2004. Competition between biological and photochemical processes in the mineralization of dissolved organic carbon. Limnol. Oceanogr. **49**: 117–124. doi:10.4319/lo.2004.49.1.0117

Oksanen, J., and others. 2011. vegan: Community ecology package. R package version 2.0-0.

Osburn, C. L., C. R. Wigdahl, S. C. Fritz, and J. E. Saros. 2011. Dissolved organic matter composition and photoreactivity in prairie lakes of the U.S. Great Plains. Limnol. Oceanogr. **56**: 2371–2390. doi:10.4319/lo.2011.56.6.2371

Osburn, C. L., and others. 2017. Shifts in the source and composition of dissolved organic matter in Southwest Greenland lakes along a regional hydro-climatic gradient. J. Geophys. Res. Biogeosci. **122**: 3431–3445. doi:10.1002/2017jg003999

Osterholz, H., D. L. Kirchman, J. Niggemann, and T. Dittmar. 2016. Environmental drivers of dissolved organic matter molecular composition in the Delaware Estuary. Front. Earth Sci. **4**: 95. doi:10.3389/feart.2016.00095

Pace, M., and others. 2004. Whole-lake carbon-13 additions reveal terrestrial support of aquatic food webs. Nature **427**: 240–243. doi:10.1038/nature02227

Poulin, B. A., J. N. Ryan, and G. R. Aiken. 2014. Effects of iron on optical properties of dissolved organic matter. Environ. Sci. Technol. **48**: 10098–10106. doi:10.1021/es502670r

R Core Team. 2015. R: A language and environment for statistical computing. R Foundation for Statistical Computing.

Raymond, P. A., and others. 2007. Flux and age of dissolved organic carbon exported to the Arctic Ocean: A carbon isotopic study of the five largest arctic rivers. Global Biogeochem. Cycles **21**: GB4011. doi:10.1029/2007gb002934

Raymond, P. A., J. E. Saiers, and W. V. Sobczak. 2016. Hydrological and biogeochemical controls on watershed dissolved organic matter transport: Pulse-shunt concept. Ecology **97**: 5–16. doi:10.1890/14-1684.1

Rivas-Ubach, A., Y. Liu, T. S. Bianchi, N. Tolic, C. Jansson, and L. Pasa-Tolic. 2018. Moving beyond the van Krevelen Diagram: A new stoichiometric approach for compound classification in organisms. Anal. Chem. **90**: 6152–6160. doi:10.1021/acs.analchem.8b00529

Rossel, P. E., A. Stubbins, P. F. Hach, and T. Dittmar. 2015. Bioavailability and molecular composition of dissolved organic matter from a diffuse hydrothermal system. Mar. Chem. **177**: 257–266. doi:10.1016/j.marchem.2015.07.002

Saros, J. E., and others. 2015. Recent decrease in DOC concentrations in Arctic lakes of southwest Greenland. Geophys. Res. Lett. **42**: 6703–6709. doi:10.1002/2015GL065075

Scribner, C. A., E. E. Martin, J. B. Martin, K. M. Deuerling, D. F. Collazo, and A. T. Marshall. 2015. Exposure age and climate controls on weathering in deglaciated watersheds of western Greenland. Geochim. Cosmochim. Acta **170**: 157–172. doi:10.1016/j.gca.2015.08.008

Seekell, D. A., and others. 2015. The influence of dissolved organic carbon on primary production in northern lakes. Limnol. Oceanogr. **60**: 1276–1285. doi:10.1002/lno.10096

Sleighter, R. L., and others. 2014. Evidence of incorporation of abiotic S and N into prairie wetland dissolved organic matter. Environ. Sci. Technol. Lett. **1**: 345–350. doi:10.1021/ez500229b

Spencer, R. G. M., G. R. Aiken, K. P. Wickland, R. G. Striegl, and P. J. Hernes. 2008. Seasonal and spatial variability in dissolved organic matter quantity and composition from the Yukon River basin, Alaska. Global Biogeochem. Cycles **22**: GB4002. doi:10.1029/2008GB003231

Spencer, R. G. M., G. R. Aiken, K. D. Butler, M. M. Dornblaser, R. G. Striegl, and P. J. Hernes. 2009. Utilizing chromophoric dissolved organic matter measurements to derive export and reactivity of dissolved organic carbon exported to the Arctic Ocean: A case study of the Yukon River, Alaska.

Geophys. Res. Lett. **36**: L06401. doi:10.1029/2008GL036831

Spencer, R. G. M., K. D. Butler, and G. R. Aiken. 2012. Dissolved organic carbon and chromophoric dissolved organic matter properties of rivers in the USA. J. Geophys. Res. **117**: G03001. doi:10.1029/2011JG001928

Spencer, R. G. M., and others. 2013. Chromophoric dissolved organic matter export from U.S. rivers. Geophys. Res. Lett. **40**: 1575–1579. doi:10.1002/grl.50357

Spencer, R. G. M., and others. 2014. Source and biolability of ancient dissolved organic matter in glacier and lake ecosystems on the Tibetan Plateau. Geochim. Cosmochim. Acta **142**: 64–74. doi:10.1016/j.gca.2014.08.006

Spencer, R. G. M., and others. 2015. Detecting the signature of permafrost thaw in Arctic rivers. Geophys. Res. Lett. **42**: 2830–2835. doi:10.1002/2015GL063498

Stedmon, C. A., S. Markager, L. Tranvik, L. Kronberg, T. Slätis, and W. Martinsen. 2007. Photochemical production of ammonium and transformation of dissolved organic matter in the Baltic Sea. Mar. Chem. **104**: 227–240. doi:10.1016/j.marchem.2006.11.005

Stedmon, C. A., R. M. W. Amon, A. J. Rinehart, and S. A. Walker. 2011. The supply and characteristics of colored dissolved organic matter (CDOM) in the Arctic Ocean: Pan Arctic trends and differences. Mar. Chem. **124**: 108–118. doi:10.1016/j.marchem.2010.12.007

Stenson, A. C., A. G. Marshall, and W. T. Cooper. 2003. Exact masses and chemical formulas of individual Suwannee River fulvic acids from ultrahigh resolution electrospray ionization Fourier transform ion cyclotron resonance mass spectra. Anal. Chem. **75**: 1275–1284. doi:10.1021/ac026106p

Stubbins, A., and others. 2010. Illuminated darkness: Molecular signatures of Congo River dissolved organic matter and its photochemical alteration as revealed by ultrahigh precision mass spectrometry. Limnol. Oceanogr. **55**: 1467–1477. doi:10.4319/lo.2010.55.4.1467

Stubbins, A., and T. Dittmar. 2015. Illuminating the deep: Molecular signatures of photochemical alteration of dissolved organic matter from North Atlantic Deep Water. Mar. Chem. **177**: 318–324. doi:10.1016/j.marchem.2015.06.020

Stubbins, A., and others. 2017. Low photolability of yedoma permafrost dissolved organic carbon. J. Geophys. Res. Biogeosci. **122**: 200–211. doi:10.1002/2016JG003688

Sun, L., E. M. Perdue, J. L. Meyer, and J. Weis. 1997. Use of elemental composition to predict bioavailability of dissolved organic matter in a Georgia river. Limnol. Oceanogr. **42**: 714–721. doi:10.4319/lo.1997.42.4.0714

Traina, S. J., J. Novak, and N. E. Smeck. 1990. An ultraviolet absorbance method of estimating the percent aromatic carbon content of humic acids. J. Environ. Qual. **19**: 151–153. doi:10.2134/jeq1990.00472425001900010023x

Vadeboncoeur, Y., E. Jeppesen, M. J. Vander Zanden, H. H. Schierup, K. Christoffersen, and D. M. Lodge. 2003. From Greenland to green lakes: Cultural eutrophication and the loss of benthic pathways in lakes. Limnol. Oceanogr. **48**: 1408–1418. doi:10.4319/lo.2003.48.4.1408

Wagner, S., T. Riedel, J. Niggemann, A. V. Vahatalo, T. Dittmar, and R. Jaffe. 2015. Linking the molecular signature of heteroatomic dissolved organic matter to watershed characteristics in world rivers. Environ. Sci. Technol. **49**: 13798–13806. doi:10.1021/acs.est.5b00525

Weishaar, J. L., G. R. Aiken, B. A. Bergamaschi, M. S. Fram, R. Fujii, and K. Mopper. 2003. Evaluation of specific ultraviolet absorbance as an indicator of the chemical composition and reactivity of dissolved organic carbon. Environ. Sci. Technol. **37**: 4702–4708. doi:10.1021/es030360x

Wiklund, J. A., R. I. Hall, and B. B. Wolfe. 2012. Timescales of hydrolimnological change in floodplain lakes of the Peace-Athabasca Delta, northern Alberta, Canada. Ecohydrology **5**: 351–367. doi:10.1002/eco.226

Wolfe, B. B., and others. 2007. Classification of hydrological regimes of northern floodplain basins (Peace–Athabasca Delta, Canada) from analysis of stable isotopes (δ^{18}O, δ^{2}H) and water chemistry. Hydrol. Process. **21**: 151–168. doi:10.1002/hyp.6229

Wünsch, U. J., K. R. Murphy, and C. A. Stedmon. 2015. Fluorescence quantum yields of natural organic matter and organic compounds: Implications for the fluorescence-based interpretation of organic matter composition. Front. Mar. Sci. **2**: 98. doi:10.3791/53408

Conflict of Interest

None declared.